1998LNP...506...83S

The Soft X-ray Background Spectrum from DXS

W.T. Sanders[1], R.J. Edgar[2], D.A. Liedahl[3], and J.P. Morgenthaler[1]

[1] Department of Physics, University of Wisconsin–Madison, 1150 University Avenue, Madison, WI 53706, USA
[2] Center for Astrophysics, 60 Garden Street, Cambridge, MA 02138, USA
[3] V-Division, Lawrence Livermore National Lab., P. O. Box 808, L–41, Livermore, CA 94550, USA

Abstract. The Diffuse X-ray Spectrometer (DXS) obtained spectra of the low energy X-ray (44 – 83 Å) diffuse background near the galactic plane from galactic longitudes $150° \lesssim l \lesssim 300°$ with $\lesssim 3$ Å spectral resolution and $\sim 15°$ angular resolution. Thus, DXS measured X-ray spectra that arise almost entirely from within the Local Bubble. The DXS spectra show emission lines and emission-line blends, indicating that the source of the X-ray emission is thermal – hot plasma in the Local Bubble. The measured spectra are not consistent with those predicted by standard coronal models, either with solar abundances or depleted abundances, over the temperature range $10^5 - 10^7$ K. The measured spectra are also inconsistent with the predictions of various non-equilibrium models. A nearly acceptable fit to DXS spectra can be achieved using a hybrid model that combines the Raymond & Smith ionization balance calculation with recently calculated (by DAL) ionic emission lines.

1 The Diffuse X-ray Spectrometer (DXS)

The Diffuse X-ray Spectrometer (DXS) consists of a pair of identical Bragg-crystal spectrometers that were built by our research group at the University of Wisconsin-Madison and flown by NASA as an attached Shuttle payload in January 1993. It is designed to obtain spectra of the soft X-ray background in the 150 – 284 eV (83 – 44 Å) range with ~ 2.7 Å spectral resolution and 15° (FWHM) angular resolution. Each DXS instrument, one on the Port side of the shuttle and one on the Starboard side, uses a curved crystal panel to Bragg-reflect incident soft X-rays towards a collimated position-sensitive proportional counter. The collimator allows each position along the counter to "see" a restricted piece of the curved crystal panel, and each position sees its piece of the crystal panel at a different angle. Thus, each position along the counter sees a different wavelength x-ray from a different direction on the sky than does its neighboring position. By rotating the counter about an axis perpendicular to the dispersion direction of the crystals through an angle of $\sim 60°$, X-rays from one direction are successively reflected across the face of the proportional counter, so that a complete spectrum over the 150 – 284 eV

© Springer-Verlag Berlin Heidelberg 1998 • Provided by the NASA Astrophysics Data System

1998LNP...506...83S

range from that direction is obtained. The DXS instruments are described more fully by Sanders et al. (1992).

2 DXS Calibration

The DXS post-flight laboratory calibrations measured the instrument area-solid angle product using three fluorescent lines: the carbon K-alpha line (277 eV), the boron K-alpha line (183 eV) and the zirconium M-zeta line (151 eV). Figure 1 shows the almost-final DXS area-solid angle product as a function of energy that was used for the fits presented here. The three post-flight calibration points are indicated.

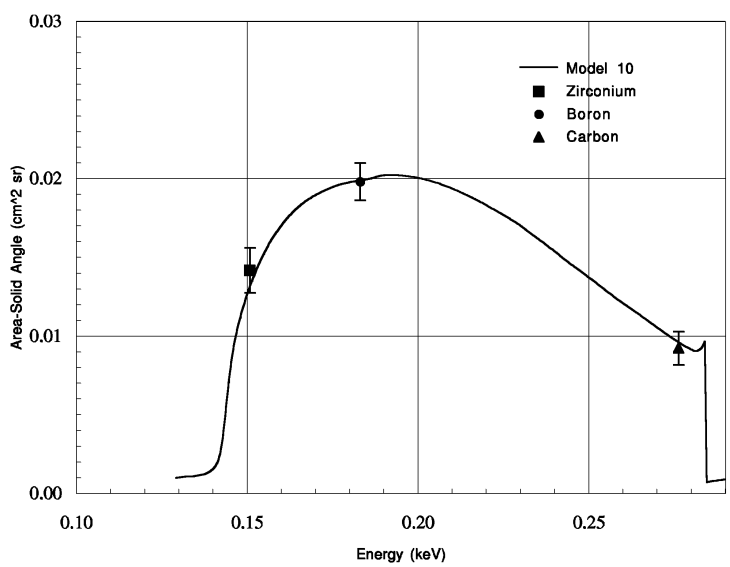

Fig. 1. Effective area - solid angle product of the DXS response function vs. energy shown with three measured calibration points.

The same laboratory calibration data were also used to determine the DXS energy scale. Bragg crystal rocking curves measured at the University of Wisconsin-Madison Synchrotron Radiation Center were used to determine the shapes of the DXS response to narrow lines. Figure 2 shows the combined laboratory data, and the DXS response function predicted output to an input model that consists of three zero-width lines at the energies indicated in parentheses. The energy scale appears to be good to ± 0.5 eV, and the widths of the laboratory fluorescent lines are greater than zero.

© Springer-Verlag Berlin Heidelberg 1998 • Provided by the NASA Astrophysics Data System

1998LNP...506...83S

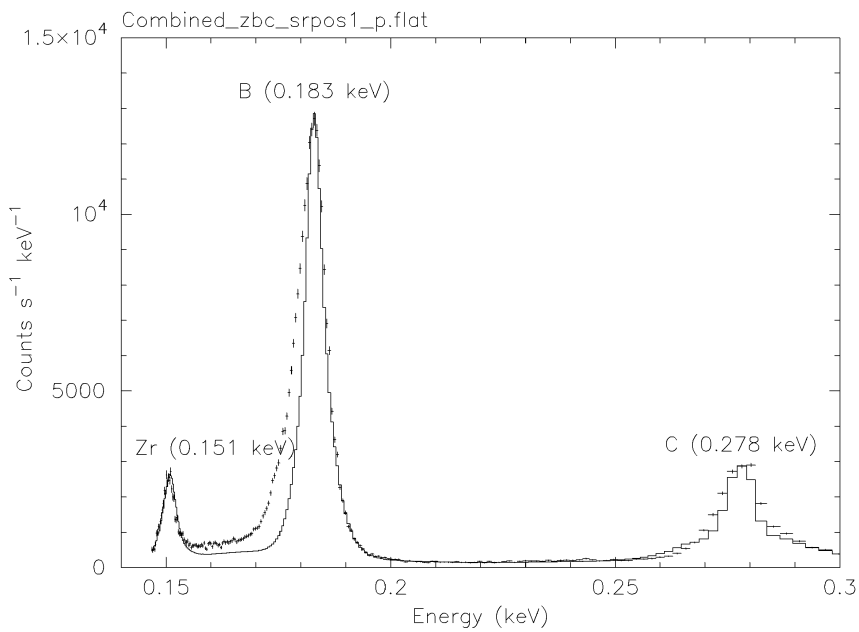

Fig. 2. Spectrum of the DXS calibration data. The solid line gives the calculated output of the DXS response function to a model of three zero-width lines at the energies in parentheses.

3 Uniqueness of the DXS Data

What is unique about the DXS data is its good spectral resolution in the 0.15 – 0.28 keV band. DXS is sensitive only in the 0.15 - 0.28 keV band, but this band, is where the Local Bubble X-ray emission is primarily seen. The DXS spectral resolution is roughly constant, $\sim$ 2.7 Å, across its 43 - 83 Å bandpass, giving it fifteen independent spectral resolution elements across the 1/4 keV band, compared to about one for a proportional counter. The DXS energy resolution ranges from $\delta E = 5$ eV at 150 eV to $\delta E = 18$ eV at 284 eV. The drawback to the DXS approach is that the efficiency of Bragg reflection low, only 1-2%, so that a long integration time or a large field of view is required. The DXS field of view was large to get reasonable statistical precision on a shuttle flight of a few days.

4 The DXS Sky Coverage

During the 80 orbit nights of DXS data collection time during the shuttle mission, the Orbiter was oriented such that the DXS detectors repeatedly scanned the same arc on the sky – an arc within 10° of the Galactic plane from longitudes 150° - 300°. The sky covered by this arc divides into five distinct regions based on count rate: Auriga (174° $\lesssim l \lesssim$ 189°), MonoGem

© Springer-Verlag Berlin Heidelberg 1998 • Provided by the NASA Astrophysics Data System

1998LNP...506...83S

($189° \lesssim l \lesssim 212°$), Puppis ($212° \lesssim l \lesssim 252°$), Vela ($252° \lesssim l \lesssim 277°$), and Crux ($277° \lesssim l \lesssim 300°$). Towards Vela, half the measured counts are due to the Vela supernova remnant, and toward the MonoGem region, a quarter of the counts are due to the MonoGem Bubble, so only toward the Auriga, Puppis, and Crux directions are we seeing featureless diffuse background from the Local Hot Bubble. The DXS Auriga spectrum is from the direction of the Taurus-Auriga dark cloud complex, a high-column density interstellar cloud whose distance is ~100 pc, whereas the DXS Puppis spectrum is from the direction without significant amounts of interstellar matter for a distance of several hundred pc. The fits presented here are to data from the Puppis direction. The Auriga and Crux spectra are similar to the Puppis spectrum, but their similarities and differences are discussed elsewhere (Morgenthaler 1997).

5 DXS Spectral Fitting

Figure 3 shows the DXS Puppis spectrum in photon units as a function of energy. Subsequent spectral fits here present the data in units of counts s^{-1} $Å^{-1}$ as a function of wavelength, because those are more natural units for these data. They are plotted with decreasing wavelength for easier comparison to the energy scale plot. Although typically we would use a 3-component spectral model to fit the diffuse background spectrum at high latitudes over the spectral range 0.1 - 1 keV, only one of those three components is useful for fitting spectra from low latitudes over the spectral range 0.15 - 0.28 keV – the unabsorbed million-degree thermal component that represents emission from the Local Bubble.

First we compare the Puppis spectrum to the model by Raymond & Smith (R&S; 1977, and subsequent updates) of a solar-abundance plasma in ionization equilibrium. The temperature and the emission measure are free parameters. As we have demonstrated previously (e.g., Sanders, Edgar, & Liedahl 1996), the best-fit parameters are similar to those found by other experiments – a temperature of $T = 1.14 \times 10^6$ K and an emission measure of $n_e^2 d = 0.0026$ cm^{-6} pc. But the value of the reduced chi-squared statistic is too large, $\sim$ 7.3 (57 degrees of freedom, hereafter, d.o.f.), so the fit is not acceptable. We also compared the Puppis spectrum to a similar model by Mewe, Kaastra, & Liedahl (MeKaL; Mewe et al. 1985, Kaastra 1992) with similar results. The best-fit temperature and emission measure are $T = 1.2 \times 10^6$ K and $n_e^2 d = 0.0029$ cm^{-6} pc, but the reduced chi-squared value is 6.0 (d.o.f. = 57), also unacceptably large. This fit is shown in Figure 4, where the solid line shows the model predictions.

There are problems with using these models to fit these data. Neither model was designed to be used to fit data with this spectral resolution, and they employ calculational approximations that may not be appropriate here. Another problem is in the atomic physics that are incorporated in these

© Springer-Verlag Berlin Heidelberg 1998 • Provided by the NASA Astrophysics Data System

1998LNP...506...83S

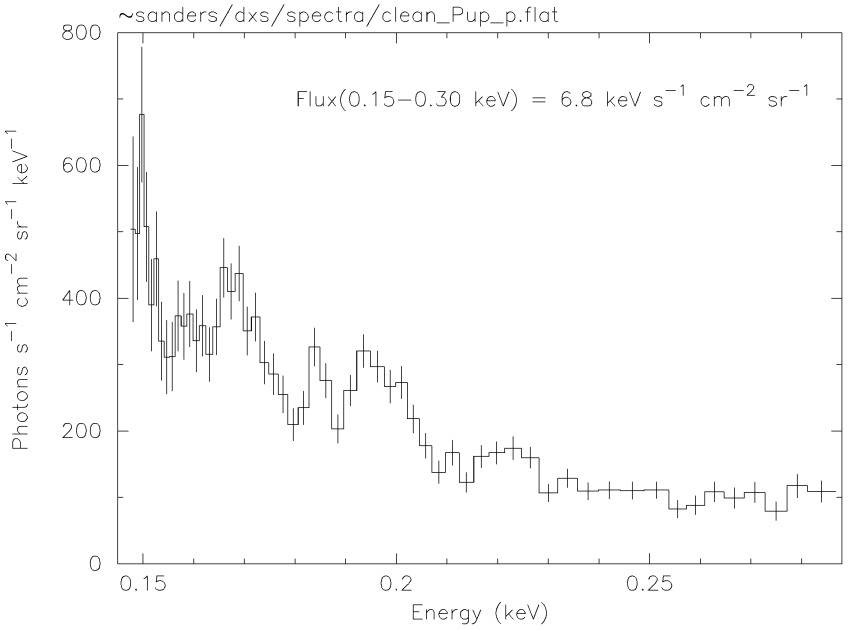

Fig. 3. DXS spectrum from the Puppis region in photon units.

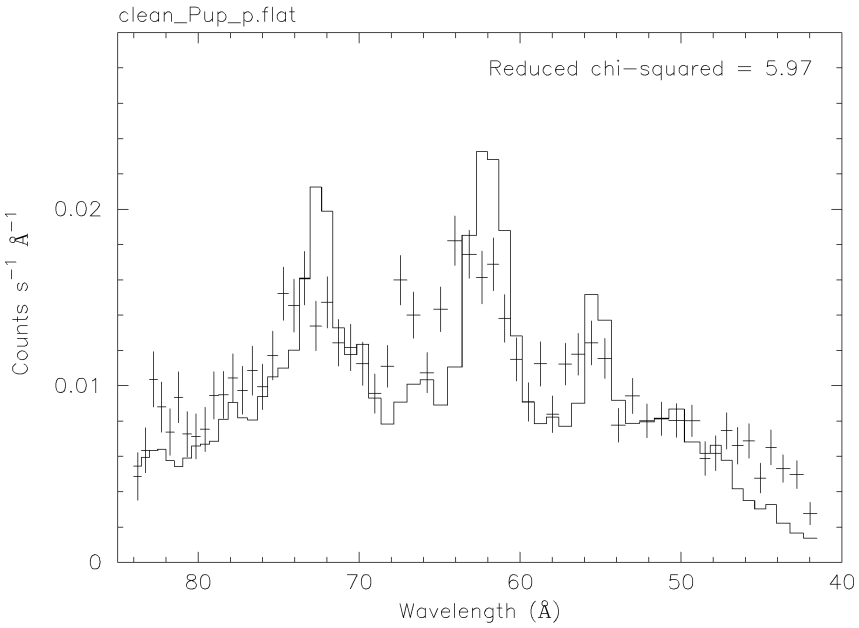

Fig. 4. Best-fit single-temperature MeKaL model to DXS Puppis data.

© Springer-Verlag Berlin Heidelberg 1998 • Provided by the NASA Astrophysics Data System

1998LNP...506...83S

models. The ionic energy levels and rates are not very well known, and again approximations are used.

We wanted to compare the DXS data to the model by Breitschwerdt & Schmutzler (1994) of the X-ray spectrum from a highly ionized plasma that experiences a delayed recombination of ions and electrons at relatively low temperatures, but we did not have a computer-compatible version of that model. We (RJE) created an approximation to that spectrum by taking a plasma that was in the ionization states of a 10^7 K plasma, and as it cooled, calculating its X-ray emission as a function of its final temperature and the fluence, the density-cooling time product. The best fit was for a final temperature $T = 10^6$ K, and a fluence $n_e t = 2 \times 10^{11}$ cm^{-3} s, with a reduced chi-squared of 4.4 (d.o.f. = 57). This fit is also not good, but it is better than the equilibrium spectral models and that suggests that the real Breitschwerdt & Schmutzler model should be fit when a computer compatible version becomes available.

We have reported previously (Sanders & Edgar 1995) that we have tried to fit the DXS data with both blast wave models and cooling plasma models, both with solar abundances and with depleted abundances, and have not found acceptable fits.

The next model we tried to fit was a "hybrid" model in which we (RJE) modified the Raymond & Smith code by replacing some of the emission line parameters in that code with updated ones that we (DAL) calculated at Livermore using the HULLAC code. The model is simply a solar-abundance single-temperature equilibrium plasma with improved atomic physics data. In particular, we (DAL) calculated improved emission line spectra for 27 ions that have strong emission lines in the DXS bandpass for a range of temperatures. Those ions are Fe IX-XVI, Mg VI-X, Si VI-XII, S VII-XII, and Ne VIII. For this model, the best-fit temperature and emission measure are $T = 1.12 \times 10^6$ K and $n_e^2 d = 0.0023$ cm^{-6} pc, with 3.2 for the reduced chi-squared value (d.o.f. = 57). Figure 5 shows this model compared to the data.

The final model that we fit was the hybrid model with the elemental abundances allowed to be non-solar. For this fit, the abundances of the elements Ne, Mg, Si, S, Ar, Ca, Fe, and Ni were free parameters, as well as the temperature and the emission measure. The reduced chi-squared statistic was 1.97 (d.o.f. = 49), with a best-fit temperature and emission measure of $T = 1.3 \times 10^6$ K and $n_e^2 d = 0.0037$ cm^{-6} pc. Figure 6 shows this fit. The best-fit abundances of only three elements were significantly different from solar: Si $\sim 0.1 \pm 0.3 \times$ solar, S $\sim 0.2 \pm 0.4 \times$ solar, and Fe $\sim 0.0 \pm 0.3 \times$ solar. Using the F-statistic, we find that these three parameters are the only ones that cause the reduction in chi-squared, so if only these three elements are allowed to vary, we get the same abundance reductions with a reduced chi-squared statistic of 1.79 (d.o.f = 54).

© Springer-Verlag Berlin Heidelberg 1998 • Provided by the NASA Astrophysics Data System

1998LNP...506...83S

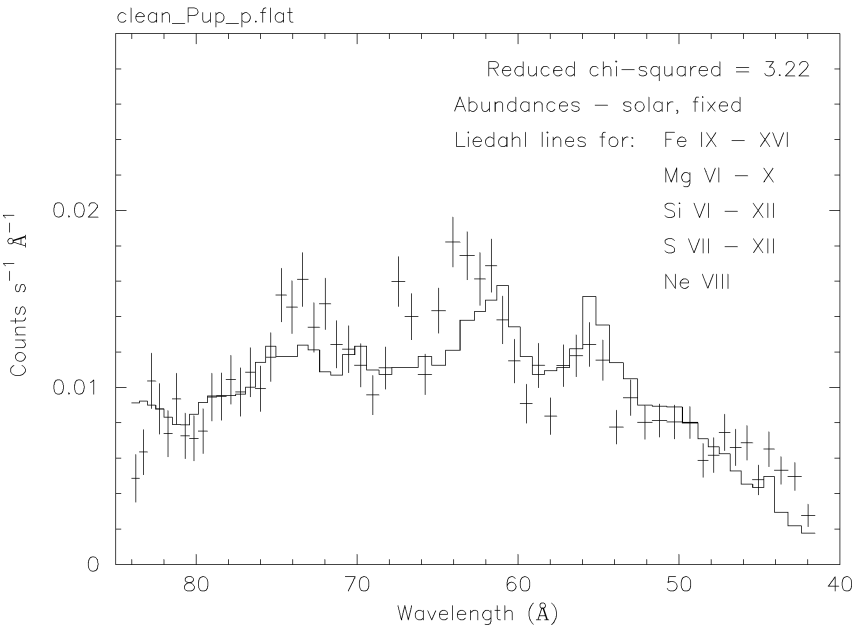

Fig. 5. Hybrid model (R & S plus Liedahl lines) fit to DXS Puppis data. Elemental abundances are solar.

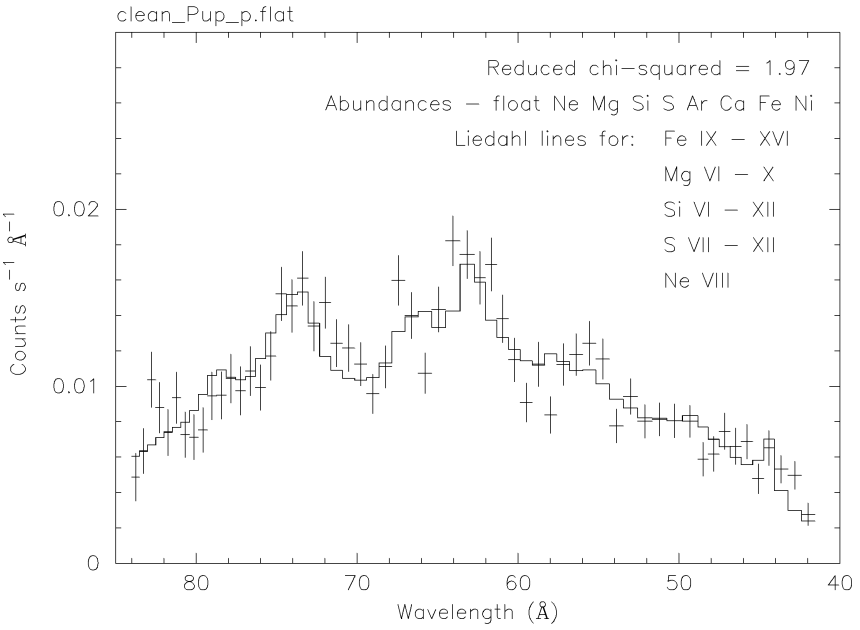

Fig. 6. Hybrid model (R & S plus Liedahl lines) fit to DXS Puppis data. Elemental abundances were allowed to float.

© Springer-Verlag Berlin Heidelberg 1998 • Provided by the NASA Astrophysics Data System

1998LNP...506...83S

If this model were a good fit, we would conclude that the abundances of Si and Fe probably are less than solar, and that the abundance of S is possibly less than solar. Interestingly, the best fit abundance for Mg is very near 1.0, whereas one might expect Mg to be also depleted, if Si and Fe were depleted. It is probably premature to speculate on the significance of a possible low abundance of Si or Fe or S, until we are more comfortable with its reality. We have concerns about the uniqueness of this solution, and about where the true minimum of chi-squared is.

6 Conclusions

1. The DXS data are consistent in intensity with previous observations of the soft X-ray background from this part of the sky.
2. The DXS spectra show clear evidence that the soft X-ray background is thermal, but "good" fits to standard models are not obtained.
3. For one particular model, the Raymond & Smith coronal plasma model, substituting the recently calculated improved ionic line spectra (by DAL) allows us to obtain significantly better fits to the DXS data.
4. Allowing the elemental abundances to deviate from solar also allows better fits to the data, but the reality and reasonableness of these "depleted" abundances is still being investigated.
5. It would be desirable to fit other standard models, such as an underionized plasma or an overionized plasma, to the DXS data, incorporating the recently calculated improved ionic line spectra.
6. Fitting the DXS data may require a model with X-ray emitting plasma at more than one temperature, as well as with non-solar elemental abundances.

References

Breitschwerdt, D., Schmutzler, T. (1994): Nature 371, 774

Kaastra, J S. (1992): An X-Ray Spectral Code for Optically Thin Plasmas (Internal SRON-Leiden Report, updated version 2.0)

Mewe, R., Gronenschild, E.H.B.M., & van den Oord, G.H.J. (1985): A&AS, 62, 197

Morgenthaler, J. P. (1997): PhD Thesis, University of Wisconsin-Madison.

Raymond, J. C. & Smith, B. W. (1977): ApJS, 35, 419

Sanders, W. T., & Edgar, R. J. (1995): in Astrophysics in the Ultraviolet, eds. S. Bowyer & R. F. Malina (Dordrecht: Kluwer), 269

Sanders, W. T., Edgar, R. J., Juda, M., Kraushaar, W. L., McCammon, D., Snowden, S. L., Zhang, J., & Skinner, M. A. (1992): Proc. of the SPIE, 1743, 60

Sanders, W. T., Edgar, R. J., & Liedahl, D. A. (1996): in Röntgenstrahlung from the Universe, eds. H. U. Zimmermann, J. E. Trümper, & H. Yorke, MPE Report 263, 339

© Springer-Verlag Berlin Heidelberg 1998 • Provided by the NASA Astrophysics Data System